Structural Basis for p19 Targeting by Anti–IL-23 Biologics: Correlations with Short- and Long-Term Efficacy in Psoriasis

Stefano G. Daniele[1,8], Sherif A. Eldirany[2,8], Giovanni Damiani[3,4,5,8], Minh Ho[6,7] and Christopher G. Bunick[6,7]

IL-23 is central to psoriasis pathogenesis. Biologics targeting IL-23 are important therapies against psoriasis. IL-23 inhibitors risankizumab, tildrakizumab, and guselkumab bind the IL-23 p19 subunit, whereas ustekinumab binds p40; however, the structural composition of the IL-23–binding epitopes and how these molecular properties relate to clinical efficacy are not known. Utilizing epitope data derived from hydrogen-deuterium exchange or crystallographic experiments, we mapped inhibitor epitope locations, hydrophobicity, and surface charge onto the IL-23 surface. Molecular properties of each inhibitor epitope, including solvent-accessible surface area, were correlated to binding affinity, kinetic values, and clinical efficacy scores for plaque psoriasis through linear regression analysis. Each IL-23 inhibitor binds an epitope with a unique size, composition, and location except for a 10-residue overlap region outside of the IL-23 receptor epitope. We observed strong correlations between epitope surface area and K_D and k_{off} but not k_{on}. Epitope surface area, K_D, and k_{off} were further associated with short-term (10–16 weeks) and long-term (44–60 weeks) clinical efficacy according to PASI-90 responses, with risankizumab demonstrating highest efficacy among IL-23 biologics. In contrast, k_{on}, epitope hydrophobicity, polarity, and charge content did not correlate with efficacy. These data exemplify how molecular principles of medications within a therapeutic class can explain their differential clinical responses.

Keywords: Inflammatory skin disease epitope, Risankizumab, Guselkumab, Tildrakizumab, Ustekinumab

JID Innovations (2024);**4:**100261 doi:10.1016/j.xjidi.2024.100261

INTRODUCTION

Psoriasis affects ~41 million people worldwide (Damiani et al, 2021), making knowledge of both its pathogenesis and treatment of paramount importance. Along with TNF-α and IL-17, IL-23 plays a central role in psoriasis pathophysiology (Chan et al, 2018). Structurally, the IL-23 cytokine is a heterodimer made of the p19 and p40 subunits, which bind IL-23 receptor (IL-23R) and IL-12Rβ1 coreceptors, respectively, to activate canonical IL-23 signaling (Figure 1a) (Glassman et al, 2021). Importantly, p19 is unique to IL-23, whereas p40 is shared among other cytokines such as IL-12 (Eldirany et al, 2020). The targeted IL-23 inhibitors—risankizumab, tildrakizumab, and guselkumab—differ mechanistically from ustekinumab because they bind specifically to p19, whereas ustekinumab binds p40, enabling both anti–IL-23 and anti–IL-12 activity. Through binding to these distinct subunits, the IL-23–targeted inhibitors and ustekinumab exert their therapeutic function by interrupting specific subunit/coreceptor interactions.

Eldirany et al (2020) previously analyzed the binding sites/epitopes of TNF-α, IL-17, and IL-23 inhibitors, identifying molecular differences among the epitopes of agents within each biologic class and possible links between epitope structure and clinical efficacy. However, the IL-23 inhibitor analysis in that study was limited to ustekinumab because structural data were lacking for other biologics. Hence, a knowledge gap exists regarding the structural mechanisms of action of the p19-specific IL-23 inhibitors in clinical use.

In this study, we characterize the molecular and structural properties of IL-23 inhibitors by analyzing experimentally derived epitope data for risankizumab, tildrakizumab, and guselkumab, in addition to those of ustekinumab. We also investigate the hypothesis that structural differences between biologic epitopes underlie variations in pharmacodynamics and short- and long-term clinical efficacy.

RESULTS

Epitope location

To compare IL-23 inhibitor binding mechanisms, each biologic epitope and IL-23R–binding site were mapped onto the

[1]*MD-PhD Program, Yale School of Medicine, New Haven, Connecticut, USA;* [2]*Department of Dermatology, University of Connecticut Health Center, Farmington, Connecticut, USA;* [3]*Italian Center of Precision Medicine and Chronic Inflammation, Milan, Italy;* [4]*Department of Biomedical, Surgical, and Dental Sciences, University of Milan, Milan, Italy;* [5]*Graduate Program (PhD) in Pharmacological Sciences, Department of Pharmaceutical and Pharmacological Sciences, University of Padua, Padua, Italy;* [6]*Department of Dermatology, Yale School of Medicine, New Haven, Connecticut, USA; and* [7]*Program in Translational Biomedicine, Yale School of Medicine, New Haven, Connecticut, USA*

[8]*These authors contributed equally to this work.*

Correspondence: Christopher G. Bunick, Department of Dermatology, Yale School of Medicine, 333 Cedar Street, LCI 501, PO Box 208059, New Haven, Connecticut 06520-8059, USA. E-mail: christopher.bunick@yale.edu

Abbreviations: IL-23R, IL-23 receptor; IXE, ixekizumab; SA, surface area; SEC, secukinumab

Received 9 August 2023; revised 6 December 2023; accepted 19 December 2023; accepted manuscript published online 20 January 2024; corrected proof published online 5 March 2024

Cite this article as: JID Innovations 2024;4:100261

© 2024 The Authors. Published by Elsevier Inc. on behalf of the Society for Investigative Dermatology. This is an open access article under the CC BY-NC-ND license (http://creativecommons.org/licenses/by-nc-nd/4.0/).

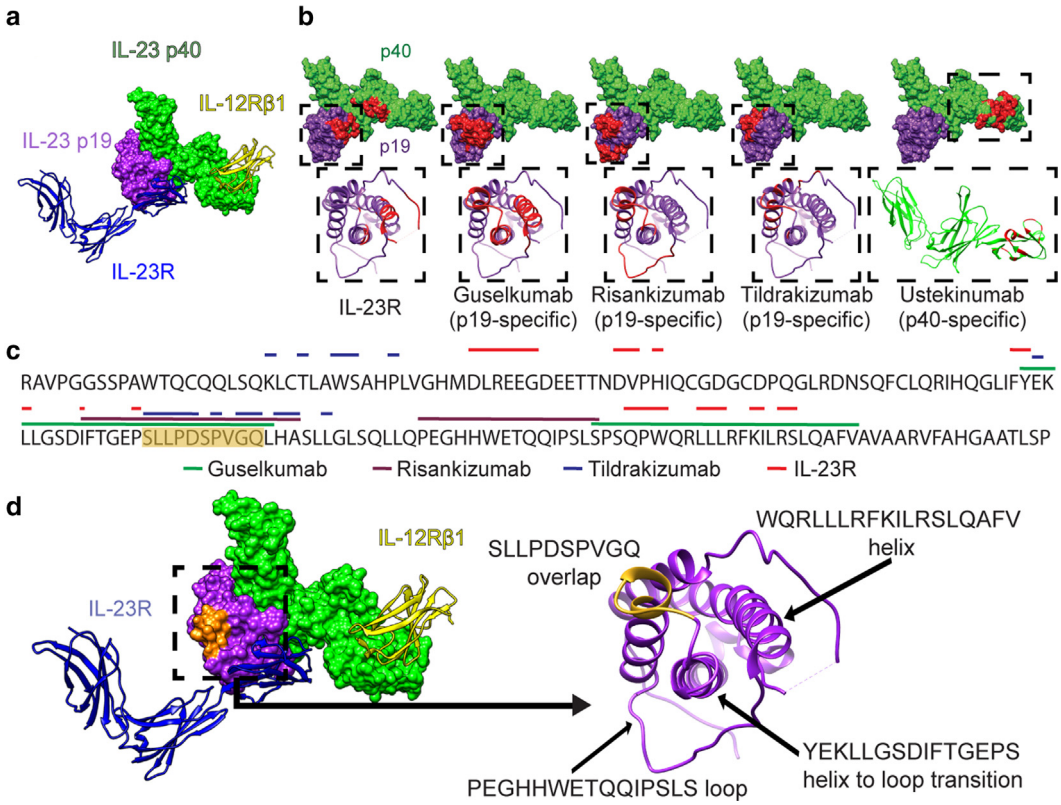

Figure 1. Structural analysis of the IL-23R complex and IL-23 inhibitor—binding locations. (**a**) Canonical IL-23 signaling consists of IL-23 p19 (purple) binding to the IL-23R receptor (blue ribbon) and the IL-23 p40 domain (green) binding to the IL-12Rβ1 receptor (yellow ribbon). Noncanonical receptor activation may also occur through IL-23R—p19 interaction alone (Schröder et al, 2015). (**b**) IL-23R— and IL-23 inhibitor—binding sites shown in red on the IL-23 molecular surface (above). IL-23 p19, purple; IL-23 p40, green. Ribbon structures (below) of boxed areas (above) of the p19 or p40 subunits with epitopes colored red. (**c**) The amino acid sequence of the IL-23 p19 subunit (R20 through P189) is shown, with overlying lines corresponding to IL-23R and drug-binding sites (ustekinumab is not included because it binds p40). The sequence S114—Q123 containing significant epitope overlap among the IL-23 inhibitors is colored orange, notably in an area that is not a direct IL-23R target. (**d**) IL-23 molecule (left) and ribbon structures of the IL-23R receptor (blue) and of the IL-12Rβ1 receptor (yellow), with the S114—Q123 sequence highlighted from **c** in orange. p19 ribbon structure (right) is associated with the boxed area (left), demonstrating the S114—Q123 overlap and other loop and helix secondary structures of p19 that define important epitope components for inhibitors in **b** and **c**. IL-23R, IL-23 receptor; SA, surface area.

molecular surface of IL-23 (Figure 1b). Risankizumab, tildrakizumab, and guselkumab epitopes exist exclusively on p19, whereas ustekinumab binds exclusively on p40. Risankizumab (2400 Å^2) has the largest epitope surface area (SA), followed by guselkumab (2240 Å^2), whereas ustekinumab (1390 Å^2) and tildrakizumab (1290 Å^2) bind a significantly smaller epitope SA. We find that p19-specific inhibitor epitopes differ in location, with guselkumab having the most overlap with the IL-23R—binding site. Specifically, of 24 residues comprising the IL-23R epitope, guselkumab overlaps with 58% of residues (14 of 24), risankizumab overlaps with 8% (2 of 24), and tildrakizumab overlaps with 0% (Figure 1b and c). One region exists in the IL-23 p19 sequence where all 3 epitopes overlap: 10 residues from S114—Q123 (SLLPDSPVGQ) (Figure 1c and d). Importantly, this area does not overlap with the IL-23R—binding site, suggesting that steric effects—rather than direct competition for the receptor-binding site—are sufficient to disrupt IL-23R binding.

Epitope chemistry

We next investigated whether IL-23 inhibitor epitopes had similar or different chemical compositions; the drug epitopes demonstrated a greater hydrophobic character than the IL-23R—binding site (32% hydrophobic) (Figure 2a and b). Tildrakizumab was the only drug with an epitope having a majority hydrophobic solvent accessible SA (56%), whereas guselkumab, risankizumab, and ustekinumab have epitopes with >50% nonhydrophobic residues (polar, acidic, or basic) (Figure 2b). Of the p19 epitopes, risankizumab is the only one with a strongly acidic surface charge, whereas tildrakizumab and guselkumab are net neutral owing to relatively even acidic and basic charge distributions (Figure 2b and c). On p40, ustekinumab has a strongly acidic epitope (Figure 2b and c). For comparison, IL-23R binds a largely neutral surface on p19 but a more acidic region on p40 (Figure 2c).

Correlation of epitope SA with binding affinity and kinetics

To examine whether each inhibitor's epitope SA correlated with its previously reported binding affinity and kinetic values, as measured by surface plasmon resonance (Zhou et al, 2021), we performed linear regression analysis. We observed an inverse relationship between epitope SA and an inhibitor's dissociation equilibrium constant (K_D) (Figure 3a and d) ($R^2 = 0.9772$, $P = .0115$), indicating that increased epitope SA correlates with higher epitope-binding affinity.

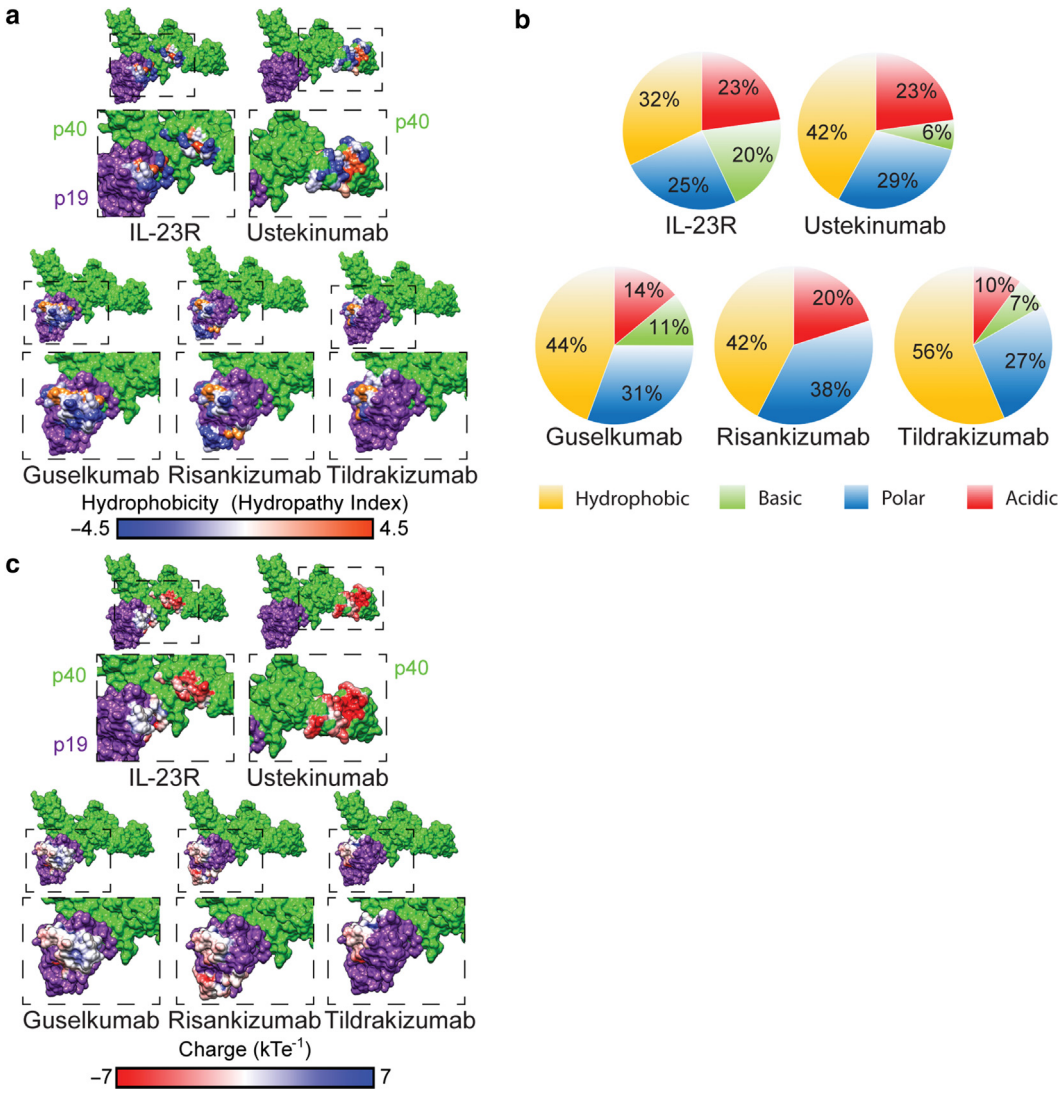

Figure 2. IL-23 inhibitor epitope characteristics. (**a**) Epitope surface hydrophobicity mapped onto IL-23. Polar epitope surfaces are shown in blue, neutral are shown in white, and hydrophobic are shown in orange. The corresponding areas of the dashed boxes (above) are enlarged below. (**b**) Proportion of each total epitope solvent-accessible SA made up of acidic, basic, polar, or hydrophobic amino acids. (**c**) Epitope surface charges mapped onto IL-23. Acidic epitope surfaces are shown in red, neutral are shown in white, and basic are shown in blue. (**a, c**) IL-23 p19 (purple) and IL-23 p40 (green). The corresponding areas of the dashed boxes (above) are enlarged below. IL-23R, IL-23 receptor; SASA, solvent-accessible surface area.

Importantly, individual epitope SA was also inversely correlated with an inhibitor's dissociation rate constant (k_{off}) (Figure 3b and d) (R^2 = 0.9489, P = .0259), whereas this same relationship was not observed between epitope SA and association rate constant (k_{on}) (Figure 3c and d) (R^2 = 0.4330, P = .3420). Therefore, these results indicate that a larger epitope SA creates more stable immune complexes with IL-23.

Correlation of epitope molecular properties with short-term clinical response

We reasoned that more stable biologic–IL-23 complexes should translate to greater clinical efficacy for plaque psoriasis. A meta-analysis comparing IL-23 inhibitor efficacy showed that risankizumab demonstrated the highest PASI-90 response rates, followed by guselkumab and ustekinumab, whereas tildrakizumab had a lower rate of achieving PASI-90 after 10–16 weeks (Armstrong et al, 2020). To examine the link between epitope structure and clinical response for IL-23 inhibitors, we compared the meta-analysis data (Table 1) with the structural properties of each inhibitor epitope identified in our analyses. We observed a stark correlation between epitope SA of each biologic and short-term (10–16 weeks) PASI-90 rates: biologics with higher epitope SA (risankizumab and guselkumab) demonstrated higher short-term PASI-90 response rates, whereas tildrakizumab, which exhibits the smallest epitope SA, exhibited the lowest rate of PASI-90 over the same timeframe (Figure 4a and Table 1) (R^2 = 0.9969, P = .0016). Notably, ustekinumab fits within this trend, indicating that ustekinumab's dual IL-12/IL-23 inhibition may not cause it to behave differently from the targeted IL-23 inhibitors in the short-term; rather, its initial efficacy may be due to the size of its epitope SA. As expected, increased binding affinity (K_D) also translated to higher PASI-90 rates (Figure 4b) (R^2 = 0.9908, P = .0046). Importantly, k_{off} also strongly correlated with PASI-90 rates (Figure 4c) (R^2 = 0.9240, P = .0387) in

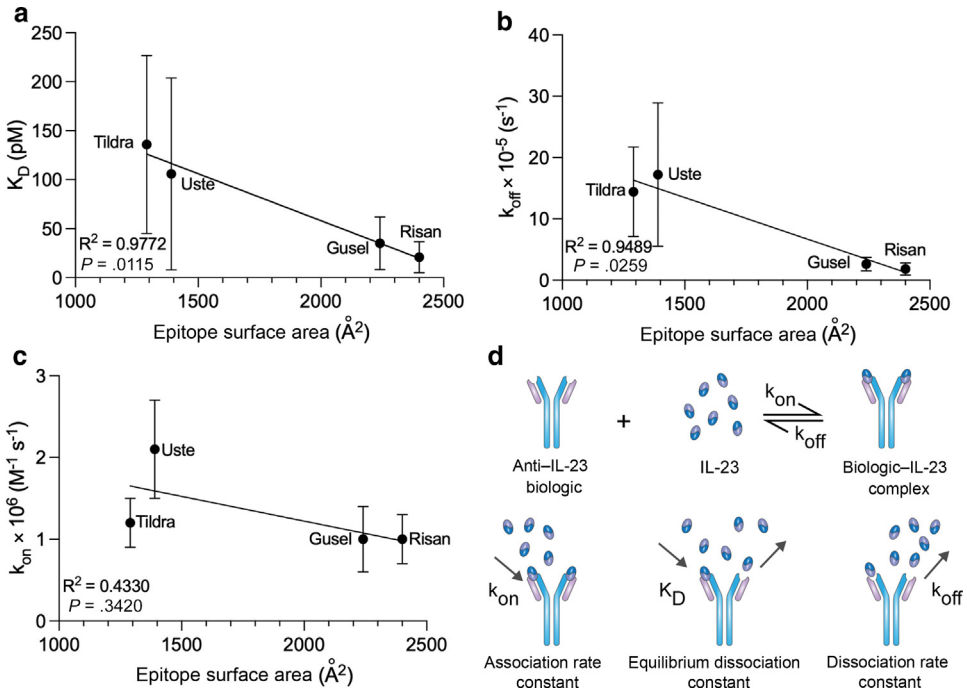

Figure 3. Correlation of IL-23 inhibitor epitope surface area with binding affinity and kinetics. (**a**) IL-23 inhibitor epitope surface area is inversely correlated with mean equilibrium dissociation constant (K_D). (**b**) Epitope surface area is also inversely correlated with mean inhibitor dissociation rate constant (k_{off}). (**c**) Epitope surface area is not correlated with mean inhibitor association rate constant (k_{on}). (**d**) Diagrammatic representation depicting antibody–antigen binding affinity and kinetics. tildra: epitope surface area = 1290 Å^2, mean K_D = 136 ± 91 pM, k_{off} = 14.4 ± 7.3 × 10^{-5} s^{-1}, k_{on} = 1.2 ± 0.3 × 10^6 M^{-1} s^{-1}; uste: epitope surface area = 1390 Å^2, mean K_D = 106 ± 98 pM, k_{off} = 17.2 ± 11.7 × 10^{-5} s^{-1}, k_{on} = 2.1 ± 0.6 × 10^6 M^{-1} s^{-1}; gusel: epitope surface area = 2240 Å^2, mean K_D = 35 ± 27 pM, k_{off} = 2.6 ± 1.1 × 10^{-5} s^{-1}, k_{on} = 1.0 ± 0.4 × 10^6 M^{-1} s^{-1}; and risan: epitope surface area = 2400 Å^2, mean = K_D 21 ± 16 pM, k_{off} = 1.8 ± 1.0 × 10^{-5} s^{-1}, and k_{on} = 1.0 ± 0.3 × 10^6 M^{-1} s^{-1}. Error bars represent SD. K_D, k_{off}, k_{on}, and SD values are derived from the study by Zhou et al (2021). gusel, guselkumab; IL-23R, IL-23 receptor; risan, risankizumab; tildra, tildrakizumab; uste, ustekinumab.

contrast to k_{on} (Figure 4d) (R^2 = 0.3796, P = .3839), indicating that slower dissociation of biologic–IL-23 complex leads to more effective treatment of plaque psoriasis. Total residue hydrophobicity (Figure 4e) (R^2 = 0.3941, P = .3722), polarity (Figure 4f) (R^2 = 0.7369, P = .1416), and charge content (Figure 4g) (R^2 = 0.005, P = .9779) did not correlate with clinical efficacy as measured by PASI-90 rates.

Correlation of epitope molecular properties with long-term clinical response

We next investigated whether IL-23 inhibitor epitope SA, K_D, and k_{off} also correlated with long-term PASI-90 responses. To maintain analytical consistency, we utilized long-term clinical efficacy data from the same meta-analysis reporting the short-term efficacy results (Armstrong et al, 2020). However, in that study, tildrakizumab was not included in the long-term data and therefore was excluded in the subsequent analyses in this study. Similar to short-term PASI-90 responses, we observed a strong correlation between epitope SA of each biologic and long-term (44–60 weeks) PASI-90 rates (Figure 5a and Table 1) (R^2 = 0.9982, P = .0273). Inhibitor K_D (Figure 5b) (R^2 = 0.9976, P = .0313) and k_{off} (Figure 5c) (R^2 = 0.9965, P = .0375) also associated with long-term PASI-90 rates. Although long-term PASI-90 response rates

Table 1. Short-Term and Long-Term PASI-90 and PASI-100 Response Rates, along with Epitope Surface Area for Anti–IL-23 Biologics

Biologic	Short-Term PASI-90 Response Rate %, 95% CI	Long-Term PASI-90 Response Rate %, 95% CI	Short-Term PASI-100 Response Rate %, 95% CI	Long-Term PASI-100 Response Rate %, 95% CI	Epitope Surface Area (Å^2)
Risankizumab (150 mg)	71.6 (67.5–75.4)	79.4 (75.5–82.9)	40.4 (35.9–45.0)	56.2 (52.4–59.9)	2400
Guselkumab (100 mg)	67.3 (62.5–71.9)	76.3 (71.4–80.6)	35.7 (30.9–40.7)	47.4 (42.1–52.8)	2240
Ustekinumab (45 mg ≤ 100 kg or 90 mg > 100 kg)	43.9 (40.2–47.9)	52.4 (47.1–57.7)	16.7 (14.4–19.3)	31.0 (27.2–35.2)	1390
Tildrakizumab (200 mg)	38.8 (33.3–44.7)	—	13.6 (10.6–17.1)	—	1290

Abbreviations: CI, confidence interval; NMA, network meta-analysis; NRI, nonresponder imputation.

Short-term (10–16 weeks) PASI-90 and PASI-100 data were reported in the study by Armstrong et al (2020). Long-term (44–60 weeks) PASI-90 and PASI-100 response rates are NRI data from eTable 3 in the study by Armstrong et al (2020). Note that long-term PASI-90 and PASI-100 for tildrakizumab are not included owing to their absence in the long-term NMA (Armstrong et al, 2020). The total numbers of patients achieving long-term PASI-90 in this NRI dataset were 714 of 899 for risankizumab, 251 of 329 for guselkumab, and 687 of 1313 for ustekinumab. The maximum numbers of evaluated patients in the entire NMA for each biologic were 1306 for risankizumab, 950 for guselkumab, 4099 for Ustekinumab, and 1413 for tildrakizumab (Armstrong et al, 2020). Please see Armstrong et al (2020) for a complete breakdown of all clinical trials included in the NMA for each biologic.

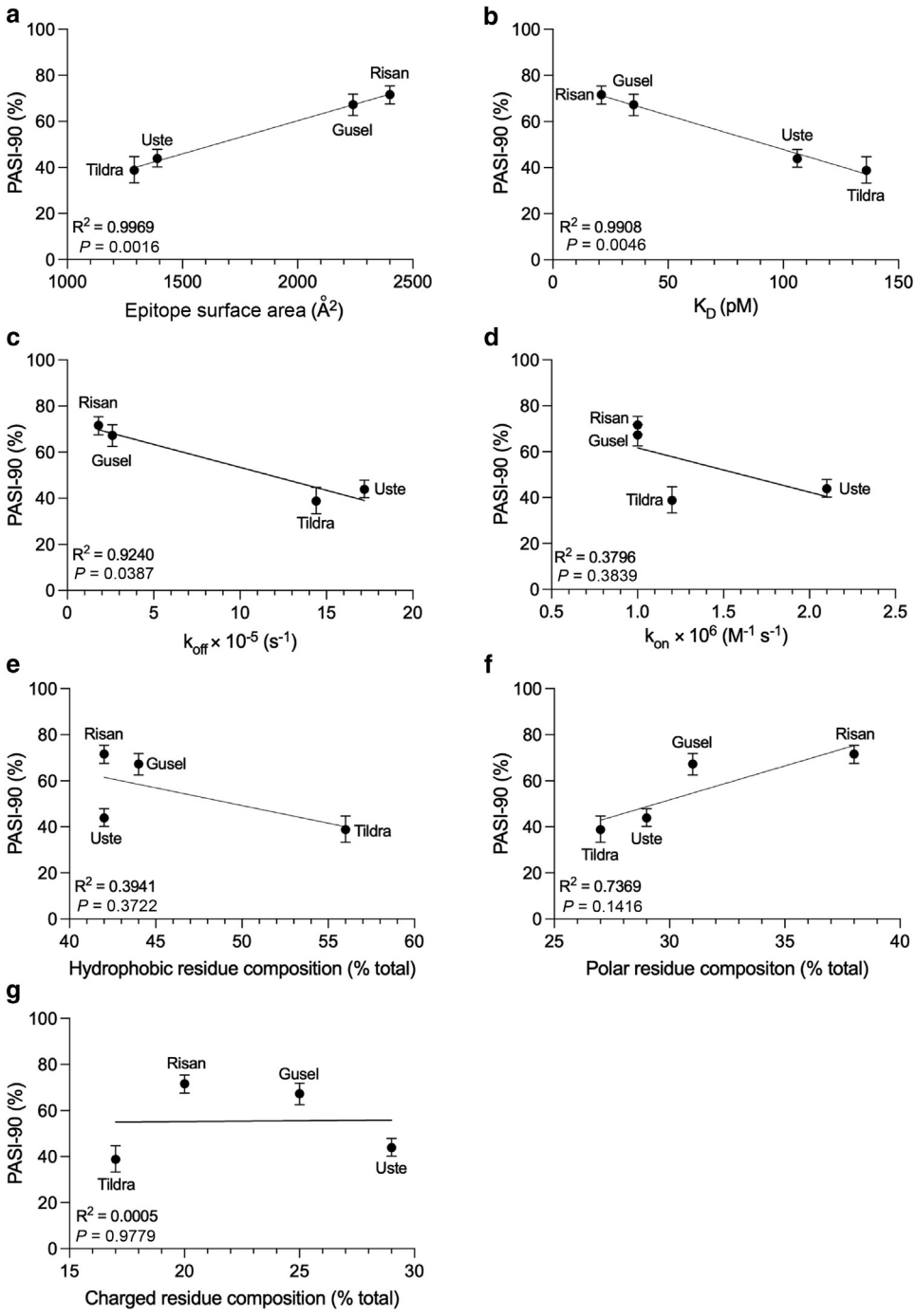

Figure 4. Correlation of IL-23 inhibitor epitope molecular properties with short-term clinical efficacy. (**a**) The efficacy of each IL-23–targeting biologic, as measured by 10–16-week PASI-90 response, is directly correlated with the size of the epitope surface area. (**b**) Mean inhibitor epitope equilibrium dissociation constant (K_D) is inversely correlated with short-term PASI-90 response. (**c**) Mean inhibitor dissociation rate constant (k_{off}) is also inversely correlated with short-term PASI-90 response rate. (**d**) Mean inhibitor association rate constant (k_{on}) is not related to short-term PASI-90 response rate. (**e**–**g**) Total residue hydrophobicity, polarity, and charge composition do not correlate with short-term PASI-90 clinical response. tildra: mean PASI-90 = 38.8% (95% CI = 33.3–44.7); gusel: mean PASI-90 = 67.3% (95% CI = 62.5–71.9); uste: mean PASI-90 = 43.9% (95% CI = 40.2–47.9); and risan: mean PASI-90 = 71.6% (95% CI = 67.5–75.4). Error bars represent upper and lower bounds of 95% CI. Mean PASI-90 and 95% CI data are derived from the study by Armstrong et al (2020). Mean K_D, k_{off}, and k_{on} values are derived from the study by Zhou et al (2021). CI, confidence interval; gusel, guselkumab; risan, risankizumab; tildra, tildrakizumab; uste, ustekinumab.

trended with k_{on}, this relationship did not reach statistical significance (Figure 5d) (R^2 = 0.9890, P = .0669). Total residue hydrophobicity (Figure 5e) (R^2 = 0.1652, P = .7336), polarity (Figure 5f) (R^2 = 0.5564, P = .4840), and charge content (Figure 5g) (R^2 = 0.5564, P = .4640) did not correlate with long-term clinical efficacy. We note that, after loading doses, risankizumab and tildrakizumab are dosed every 12 weeks whereas guselkumab is dosed every 8 weeks.

DISCUSSION

Computational structural analysis of IL-23 inhibitor epitopes revealed important molecular differences among p19-specific psoriasis biologics that have direct relevance to patient outcomes. Strong correlations between inhibitor epitope SA, binding affinity, dissociation kinetics, and PASI-90 response rates exemplify how biochemical and molecular data are critical for explaining clinical observations. Furthermore, structure–function–clinical response relationships can inform future pharmacologic innovation.

Our analyses suggest that the size/SA of the IL-23 inhibitor epitope is an important structural parameter in defining and explaining both short- and long-term therapeutic response for IL-23 biologics in plaque psoriasis treatment, more than total residue hydrophobicity, polarity, or charge content. The link

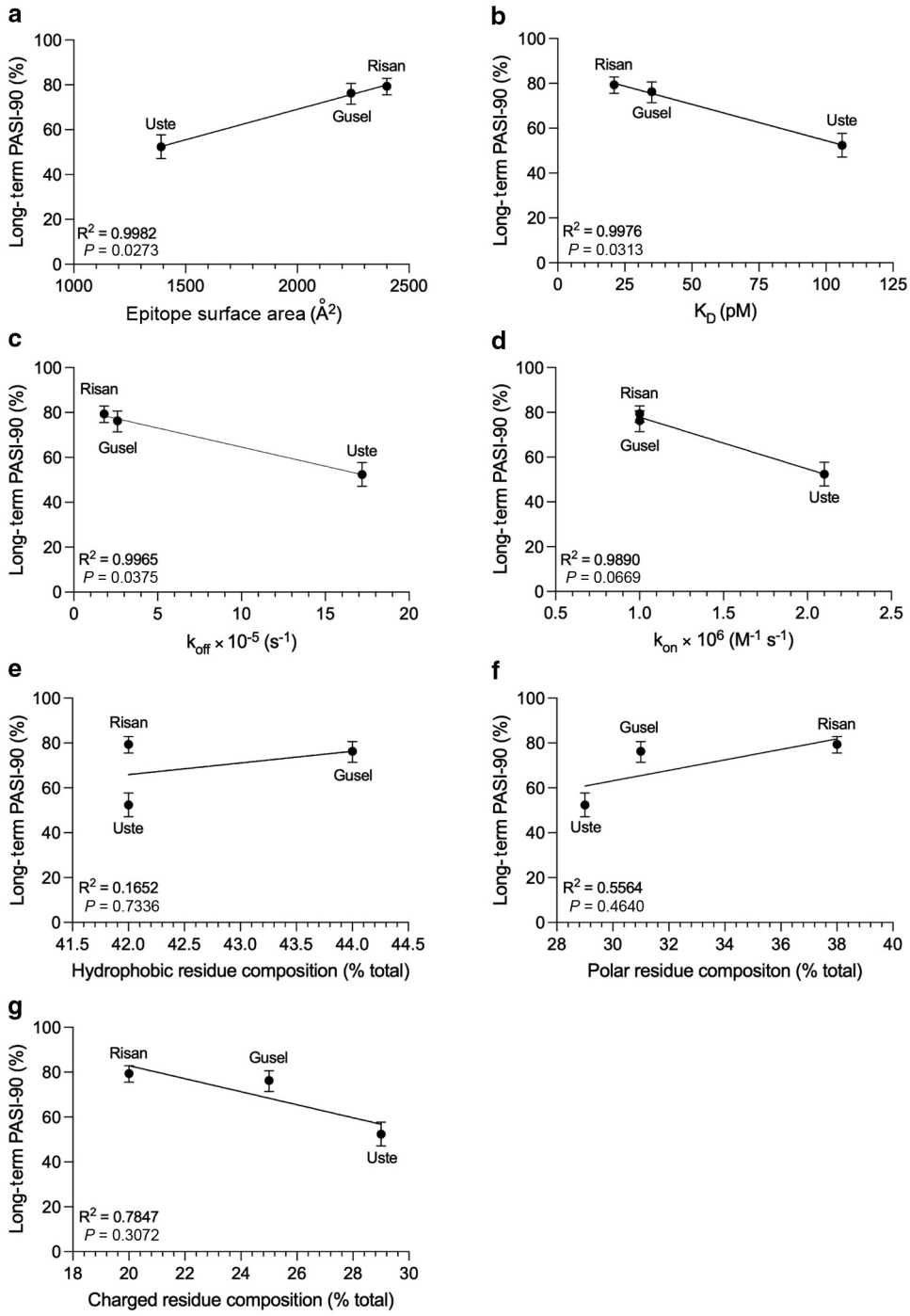

Figure 5. Correlation of IL-23 inhibitor epitope molecular properties with long-term clinical efficacy. (**a**) The efficacy of each IL-23–targeting biologic, as measured by 44–60-week PASI-90 response, is directly correlated with the size of the epitope surface area. (**b**) Mean inhibitor epitope equilibrium dissociation constant (K_D) is inversely correlated with long-term PASI-90 response. (**c**) Mean inhibitor dissociation rate constant (k_{off}) is also inversely correlated with long-term PASI-90 response rate. (**d**) Mean inhibitor association rate constant (k_{on}) is not related to long-term PASI-90 response rate. (**e**–**g**) Total residue hydrophobicity, polarity, and charge composition do not correlate with long-term PASI-90 clinical response. gusel: mean long-term PASI-90 = 76.3% (95% CI = 71.4–80.6); uste: mean long-term PASI-90 = 52.4% (95% CI = 47.1–57.7); and risan: mean long-term PASI-90 = 79.4% (95% CI = 75.5–82.9). Error bars represent upper and lower bounds of 95% CI. Mean long-term PASI-90 and 95% CI data are derived from eTable 3 (NRI data) from the study by Armstrong et al (2020). Mean K_D, k_{off}, and k_{on} values are derived from the study by Zhou et al (2021). CI, confidence interval; gusel, guselkumab; NRI, nonresponder imputation; risan, risankizumab; uste, ustekinumab.

between epitope SA and clinical response likely stems from its relationship with inhibitor-binding affinity and dissociation kinetics.

We observed a strong inverse correlation between epitope SA and K_D and epitope SA and k_{off}, both of which are also independently correlated with PASI-90 response rates. Interestingly, we did not find a significant correlation between inhibitor epitope SA and k_{on}, nor did we observe a significant relationship between k_{on} and short- or long-term clinical response, indicating that association dynamics between biologics and IL-23 are less important for clinical response. Our data ultimately indicate that epitope SA has a major influence on stable drug–target complex formation and preventing biologic–IL-23 dissociation, which mitigates aberrant IL-23 signaling central to psoriasis pathophysiology.

Our data align with previous preclinical findings examining the in vitro potency and in vivo efficacy of risankizumab, tildrakizumab, guselkumab, and ustekinumab (Zhou et al, 2021). Our work deepens the molecular understanding of IL-23 inhibitors by characterizing and differentiating the chemistry and structure of their binding epitopes. In doing so, we provide the molecular rationale underpinning not only

preclinical findings (Zhou et al, 2021) but also the short- and long-term clinical efficacy of these medications in the treatment of plaque psoriasis (Armstrong et al, 2020). Moreover, our data confirms that direct IL-23 inhibitor epitope overlap with the IL-23R epitope is not required for clinical efficacy because risankizumab and tildrakizumab demonstrate clinically meaningful PASI-90 responses despite low (8 and 0%, respectively) epitope overlap with IL-23R. We also find that each IL-23—targeted inhibitor epitope corresponds to a unique location on the IL-23 p19 subunit except for a 10-residue region from S114—Q123 (SLLPDSPVGQ). This area likewise does not overlap with the IL-23R—binding region, providing further evidence that direct interference between inhibitor and IL-23R binding is not always necessary for clinical efficacy.

Our findings regarding the relationship between epitope size/SA, k_{off}, and clinical efficacy in plaque psoriasis are not unique to IL-23 inhibitors but instead appear to be shared with other biologic classes such as the IL-17 inhibitors: ixekizumab (IXE) and secukinumab (SEC). As reported by Warren et al (2018), a greater proportion of patients with moderate-to-severe plaque psoriasis achieved PASI-90 and PASI-100 within 12 weeks of therapy with IXE in contrast to therapy with SEC as demonstrated by indirect comparison. Importantly, the increased clinical efficacy of IXE compared with that of SEC is mirrored by its greater epitope SA of 3330 $Å^2$ than that of SEC, which has an epitope SA of 1830 $Å^2$, a finding we reported previously (Eldirany et al, 2020). Therefore, the association between epitope SA and clinical efficacy is observed with IL-17 inhibitors in addition to IL-23 inhibitors. Besides larger epitope SA, further analysis of IXE reveals that it has increased binding affinity (K_D) of $1.8 \pm 1.1 \times 10^{-12}$ M for human IL-17A in comparison with SEC, which exerts a K_D of $6.0 \pm 1.6 \times 10^{-11}$ M (European Medicines Agency, 2014; Liu et al, 2016). Similar to IL-23 inhibitors, IXE also has a lower k_{off} of $1.3 \pm 0.8 \times 10^{-5}$ s^{-1} than SEC ($2.6 \pm 0.8 \times 10^{-5}$ s^{-1}) (European Medicines Agency, 2014; Liu et al, 2016). However, a unique aspect of IXE is that it also displays a greater k_{on} ($7.5 \pm 1.4 \times 10^{6}$ M^{-1} s^{-1}) than SEC ($4.3 \pm 0.6 \times 10^{5}$ $M^{-1}s^{-1}$) (European Medicines Agency, 2014; Liu et al, 2016). In terms of epitope chemical profile, IXE and SEC differ in the total percentage of polar, acidic, basic, and hydrophobic residues, with the most notable differences being that IXE has a greater percentage of polar (55 vs 46%) and basic (19 vs 10%) residues than SEC, whereas SEC has more than double the percentage of hydrophobic residues than IXE (38 vs 16%) (Eldirany et al, 2020). As such, the higher percentage of polar and basic residues, combined with a lower percentage of hydrophobic residues, may underlie IXE's enhanced k_{on}, but its greater epitope SA likely is responsible for its decreased k_{off}. However, considering that there are only 2 compounds compared, it is difficult to draw firm correlative relationships between these molecular and clinical variables. Overall, the structuro—functional relationship (also known as structurotype) between epitope SA, k_{off}, and clinical efficacy is maintained between both IL-23 and IL-17 class therapies in the treatment of plaque psoriasis.

Analyses linking the structural properties of IL-23 inhibitor epitopes to clinical efficacy are useful to clinicians by providing molecular rationale for drug selection. One example is the molecular justification for biologic intraclass switching, as opposed to interclass switching. The analysis presented in this paper demonstrates that each p19-specific medication is molecularly distinct, and therefore, lack of clinical response to one IL-23 inhibitor does not preclude clinical response to a different IL-23 inhibitor. Similarly, Eldirany et al (2020) showed molecular justification for intraclass switching among TNF-α inhibitors, where properties such as epitope location (TNF-α loop vs sheet regions), subunit bridging (single or multisubunit binding), and epitope chemistry differentiate medications in this class.

Our ability to connect structure and function is limited by the lack of detailed biologic—cytokine structures for the medications presented in this paper; this work relies mostly on biochemical, noncrystallographic data acquired from hydrogen—deuterium exchange experiments. Future studies yielding experimentally determined structures, from X-ray crystallography or cryoelectron microscopy, can improve the precision and understanding of the structural mechanisms governing biologic drug activity. The absence of long-term clinical response data for tildrakizumab in the network meta-analysis limited our ability to include this biologic in long-term efficacy analyses (Armstrong et al, 2020). Future studies aggregating both short-term and long-term data for all IL-23 biologics in the treatment of plaque psoriasis will be necessary to provide a more complete understanding of the structural properties of inhibitor epitopes and their clinical responses.

MATERIALS AND METHODS

IL-23 epitope analysis

We utilized epitope data primarily derived from hydrogen—deuterium exchange studies for risankizumab (Singh et al, 2015), tildrakizumab (Presta, 2012), and guselkumab (Zhou et al, 2021) and crystallographic data for ustekinumab (Luo et al, 2010) to map epitope locations, hydrophobicity, and surface charge onto the surface of the IL-23 crystal structure (Protein Data Bank identification code 3D87) (Beyer et al, 2008) using UCSF Chimera (Pettersen et al, 2004). The IL-23 structure contained p19 residues R20-L187. PDBePISA was used to calculate solvent-accessible SA. Total epitope characters were determined by classifying each epitope residue as acidic (D, E), basic (R, K), polar (Q, N, H, S, T, Y, C, G), or hydrophobic (A, I, L, F, V, P, M, W) and calculating each group's total contribution to epitope solvent-accessible SA.

Correlation of inhibitor epitope properties to binding affinity, kinetics, and clinical response

The molecular properties of each inhibitor epitope (ie, SA) were correlated to previously reported binding affinity and kinetics as well as clinical efficacy in plaque psoriasis through linear regression analysis. Data utilized for each analysis are described in detail in corresponding figure legends. Briefly, composite short-term (10—16 weeks) and long-term (44—60 weeks) PASI-90 response rate data were derived from the network meta-analysis performed by Armstrong et al (2020), whereas inhibitor equilibrium dissociation constant (K_D), dissociation rate constant (k_{off}), and association rate constant (k_{on}) were derived from Zhou et al (2021). Concomitant systemic medications that may affect the biologic's therapeutic effect were not used in this study.

Statistical analysis

All statistical analyses (linear regression analysis) and data plotting were performed using Prism 9 (GraphPad Software) with significance set at $P \leq .05$. Description of error bars and raw pertinent numerical data are described in detail in each figure legend.

DATA AVAILABILITY STATEMENT

Datasets related to this article can be found in the referenced publications and structure coordinates in the Protein Data Bank according to listed accession codes.

ORCIDs

Stefano G. Daniele: http://orcid.org/0000-0002-3987-1415
Sherif A. Eldirany: http://orcid.org/0000-0003-4631-1763
Giovanni Damiani: http://orcid.org/0000-0002-2390-6505
Minh Ho: http://orcid.org/0000-0001-7192-3919
Christopher G. Bunick: http://orcid.org/0000-0002-4011-8308

CONFLICT OF INTEREST

CGB has served as a consultant for AbbVie, Almirall, Amgen, Eli Lilly, Janssen, Novartis, and UCB. The remaining authors state no conflict of interest.

ACKNOWLEDGMENTS

We thank Matt Vesely (Yale University) and Jason P. Lott (Bayer) for critical review. This work was supported by the United States National Institutes of Health/National Institute of Arthritis and Musculoskeletal and Skin Diseases under award number R01 AR079428 (to CGB) and the United States National Institutes of Health/National Institute of General Medical Sciences Medical Scientist Training Grant T32GM007205 (to SGD). Aspects of this work were presented at the 2022 South Beach Symposium, Miami, FL (CGB); the 2023 International Societies for Investigative Dermatology Meeting, Tokyo, Japan (CGB); and the 2023 World Congress of Dermatology, Singapore (CGB).

AUTHOR CONTRIBUTIONS

Conceptualization: CGB; Formal Analysis: SGD, SAE, MH, GD; Supervision: CGB; Visualization: SAE, SGD, MH, CGB; Writing - Original Draft Preparation: SGD, SAE; Writing - Review and Editing: SGD, CGB, MH, GD, CGB

REFERENCES

Armstrong AW, Puig L, Joshi A, Skup M, Williams D, Li J, et al. Comparison of biologics and oral treatments for plaque psoriasis: A meta-analysis. JAMA Dermatol 2020;156:258–69.

Beyer BM, Ingram R, Ramanathan L, Reichert P, Le HV, Madison V, et al. Crystal structures of the pro-inflammatory cytokine interleukin-23 and its complex with a high-affinity neutralizing antibody. J Mol Biol 2008;382:942–55.

Chan TC, Hawkes JE, Krueger JG. Interleukin 23 in the skin: role in psoriasis pathogenesis and selective interleukin 23 blockade as treatment. Ther Adv Chronic Dis 2018;9:111–9.

Damiani G, Bragazzi NL, Karimkhani Aksut C, Wu D, Alicandro G, McGonagle D, et al. The global, regional, and national burden of psoriasis: results and insights from the global burden of disease 2019 study. Front Med (Lausanne) 2021;8:743180.

Eldirany SA, Ho M, Bunick CG. Structural basis for how biologic medicines bind their targets in psoriasis therapy. Yale J Biol Med 2020;93:19–27.

European Medicines Agency. Cosentyx. 2014. https://www.ema.europa.eu/en/medicines/human/EPAR/cosentyx. (accessed October 21, 2023).

Glassman CR, Mathiharan YK, Jude KM, Su L, Panova O, Lupardus PJ, et al. Structural basis for IL-12 and IL-23 receptor sharing reveals a gateway for shaping actions on T versus NK cells. Cell 2021;184:983–99.e24.

Liu L, Lu J, Allan BW, Tang Y, Tetreault J, Chow CK, et al. Generation and characterization of ixekizumab, a humanized monoclonal antibody that neutralizes interleukin-17A. J Inflamm Res 2016;9:39–50.

Luo J, Wu SJ, Lacy ER, Orlovsky Y, Baker A, Teplyakov A, et al. Structural basis for the dual recognition of IL-12 and IL-23 by ustekinumab. J Mol Biol 2010;402:797–812.

Pettersen EF, Goddard TD, Huang CC, Couch GS, Greenblatt DM, Meng EC, et al. UCSF Chimera–a visualization system for exploratory research and analysis. J Comput Chem 2004;25:1605–12.

Presta LG. Engineered anti-IL-23P19 antibodies. 2012. https://patents.google.com/patent/US8293883B2/en. (accessed October 21, 2023).

Schröder J, Moll JM, Baran P, Grötzinger J, Scheller J, Floss DM. Non-canonical interleukin 23 receptor complex assembly: p40 protein recruits interleukin 12 receptor beta1 via site II and induces p19/interleukin 23 receptor interaction via site III. J Biol Chem 2015;290:359–70.

Singh S, Kroe-Barrett RR, Canada KA, Zhu X, Sepulveda E, Wu H, et al. Selective targeting of the IL23 pathway: generation and characterization of a novel high-affinity humanized anti-IL23A antibody. MAbs 2015;7:778–91.

Warren RB, Brnabic A, Saure D, Langley RG, See K, Wu JJ, et al. Matching-adjusted indirect comparison of efficacy in patients with moderate-to-severe plaque psoriasis treated with ixekizumab vs. secukinumab. Br J Dermatol 2018;178:1064–71.

Zhou L, Wang Y, Wan Q, Wu F, Barbon J, Dunstan R, et al. A non-clinical comparative study of IL-23 antibodies in psoriasis. mAbs 2021;13:1964420.

This work is licensed under a Creative Commons Attribution-NonCommercial-NoDerivatives 4.0 International License. To view a copy of this license, visit http://creativecommons.org/licenses/by-nc-nd/4.0/